A mutation in *BrPRPL1* causes leaf yellowing by influencing chloroplast protein translation in Chinese cabbage

Xiaowei Ren[1, 2]*, Xing Li[1]*, Jie Li[1]*, Jindi Fan[1], Mengyao Yuan[1], Yan Li[1], Daling Feng[1], Yin Lu[1], Hao Liang[1], Xiaofei Fan[1], Lei Sun[1], Kehui Ren[1], Mengyang Liu[1#], Wei Ma[1#], Jianjun Zhao[11#]

[1] *State Key Laboratory of North China Crop Improvement and Regulation, Key Laboratory of Vegetable Germplasm Innovation and Utilization of Hebei, Collaborative Innovation Center of Vegetable Industry in Hebei, College of Horticulture, Hebei Agricultural University, Baoding 071000, China*

[2] *Department of Agriculture and Food Science, Shijiazhuang University, Shijiazhuang 050035, China*

Highlights

· The large subunit ribosomal protein L1 of the chloroplast (*BrPRPL1*) is the candidate gene of *Mut298*.

· The silencing of *BrPRPL1* results in leaf yellowing of Chinese cabbage.

· A single nucleotide change from C to T in *BrPRPL1* significantly reduces the expression of chloroplast genome-encoded proteins RbcL, PsaA, and PsaB.

Abstract

Leaf color directly influences the appearance quality and nutritional quality of leafy vegetables, determining their economic value. Here, we identify a golden leaf mutant, *Mut298*, from an ethyl methanesulfonate (EMS)-induced mutant library of Chinese cabbage. Through the approach of forward genetics, it has been demonstrated that the phenotype of *Mut298* is due to a single nucleotide substitution from C to T change glycine to arginine in the conserved domain of *BrPRPL1*, which encodes the large subunit ribosomal protein L1 of the chloroplast. Due to the *PRPL1* mutation result in embryonic lethality in *Arabidopsis*, the function of *PRPL1* in leaf development remains elusive. In this study, the mutation of *BrPRPL1* causes a substantial reduction in the expression of key chloroplast-encoded proteins (RbcL, PsaA, and PsaB), and causing abnormal chloroplast development. Moreover, the chlorophyll content and photosynthetic parameters are significantly lower in *Mut298* plants than in wild type plants, resulting in golden yellow leaves in Chinese cabbage. This study details the impact of *PRPL1* mutation on ribosome translation within chloroplasts and sets a foundation for future research into the regulatory roles of *PRPL1* in plant growth and development.

Keywords: Chinese cabbage, Mutant, Chloroplast, Gene function, Ribosome translation

1. Introduction

Genetic variations in chlorophyll and carotenoid metabolic pathways leading to leaf yellowing in plants. In the chlorophyll biosynthesis pathway, the synthesis of 5-aminolevulinic acid (ALA) and the insertion of Mg^{2+} into protoporphyrin IX are two critical steps directly affecting chlorophyll synthesis (Li *et al*. 2019). ALA, a common precursor for both chlorophyll and heme synthesis, is catalyzed by glutamyl-tRNA reductase (GluTR),

[1] [#]Correspondence Mengyang Liu, Wei Ma and Jianjun Zhao. Tel: +86-15930700300 (Jianjun Zhao), E-mail: liumengyang_7@163.com (Mengyang Liu); mawei0720@163.com (Wei Ma); yyzjj@hebau.edu.cn (Jianjun Zhao). * These authors contributed equally to this work.

while heme, as the end product, exerts feedback inhibition on GluTR activity (Zhao *et al*. 2020). A mutation in the heme oxygenase gene blocks heme degradation, leading to its accumulation. The elevated heme levels suppress ALA synthesis via negative feedback, impairing chlorophyll production and altering leaf color in pea (Linley *et al*. 2006). Magnesium chelatase is a key enzyme in chlorophyll synthesis, catalyzing the chelation of Mg^{2+} into protoporphyrin IX to form magnesium protoporphyrin IX (Papenbrock *et al*. 2000; Masuda 2008). In higher plants, this enzyme consists of three subunits: CHLI, CHLD, and CHLH (Zhao *et al*. 2020). Mutations in *CHLI* and *CHLD* cause leaf yellowing in pea (Luo *et al*. 2013). Additionally, a single nucleotide mutation in *CHLI* reduces plastid-encoded polymerase activity, disrupting chloroplast development and chlorophyll biosynthesis in *Brassica napus*, leading to leaf yellowing (Zhao *et al*. 2020). Under ABA treatment, *MdSnRK1.1* promotes *MdGLK1* protein degradation via the 26S proteasome. Consequently, *MdGLK1*-mediated transcriptional activation of *MdHEMA1 is attenuated*, suppressing chlorophyll biosynthesis in apple (Yang *et al*. 2024). Under heat stress, the upregulated expression of *ABI5* enhances its binding to *PPH* and *PAO* promoters to activate their transcription. Furthermore, heat stress promotes the interaction between *ABI5* and *MYB44* as well as ubiquitin-mediated degradation of *MYB44*, thereby relieving *MYB44*'s transcriptional repression on *PPH* and *PAO* and ultimately accelerating chlorophyll degradation (Liu *et al*. 2023).

Carotenoids, primarily comprising yellow carotenes and orange xanthophylls, significantly influence plant organ coloration (Polivka *et al*. 2010). Phytoene synthase (*PSY*), the rate-limiting enzyme in carotenoid biosynthesis, catalyzes the condensation of isopentenyl pyrophosphate to form phytoene (Cazzonelli *et al*. 2010). *PSY* expression levels directly regulate carotenoid content, thereby influencing leaf coloration (Zhao *et al*. 2020; Wang *et al*. 2021). Furthermore, phytoene desaturase (*PDS*) is another key enzyme in carotenoid metabolism. *PDS* silencing causes yellow fruit in tomato (Naing *et al*. 2019). Under high light intensity, the upregulation of *bHLH71-like*, *CaVDE*, and *LUT5*, combined with downregulated *ZEP* expression, enhances antheraxanthin and zeaxanthin accumulation. This ultimately induces leaf yellowing in pepper (Liu *et al*. 2023).

Chloroplasts, essential organelles in green plants, are integral to various biological processes such as photosynthesis, pigment biosynthesis, and amino acid production (Fu *et al*. 2022). Their functional stability influences both chlorophyll synthesis and degradation and the coloration of plant leaves. Changes in chloroplast structure and function often correlate with leaf color variations, which makes leaf color mutants crucial for studying chloroplast dynamics (Zhao *et al*. 2020; Cheng *et al*. 2022). The chloroplast genome encodes approximately 120-130 genes, including those for photosystem I (*psa*), photosystem II (*psb*), the large subunit of ribulose-1,5-bisphosphate carboxylase/oxygenase (Rubisco) (*rbcL*), the cytochrome b6f complex (*pet*), NAD(P)H dehydrogenase (*ndh*), ATP synthase (*atp*), ribosomal RNA (rRNA), transfer RNA (tRNA), and ribosomal proteins (*rpl*, *rps*), among others (Wicke *et al*. 2011). Disruptions in these proteins' expression or function can inhibit chloroplast development, alter chlorophyll metabolism, and lead to diverse leaf color phenotypes (Kusumi *et al*. 2011).

Chloroplast ribosomes, derived from cyanobacteria, play a pivotal role in synthesizing proteins encoded by the chloroplast genome (Tiller and Bock 2014; Sun and Zerges 2015). These ribosomal proteins are essential for ribosome biogenesis, chloroplast protein biosynthesis, and early chloroplast development. Mutations in these proteins can lead to translational disorders, impairing chloroplast function and consequently affecting plant growth

and development (Romani *et al*. 2012; Robles and Quesada 2022). For instance, the absence of specific plastid ribosomal proteins in *Arabidopsis* can cause various phenotypic effects ranging from embryonic lethality to reduced viability. Loss-of-function *Arabidopsis* mutants of *PRPL1* and *PRPL4* exhibit embryonic lethality, whereas *Arabidopsis PRPL11* mutants demonstrate non-lethal symptoms such as leaf yellowing and stunted growth, due to compromised mRNA translation and photosynthesis (Romani *et al*. 2012; Pesaresi *et al*. 2001). Similarly, a mutation in *SVR8*, which encodes the chloroplast ribosome large subunit L24 in *Arabidopsis*, leads to defects in chloroplast rRNA processing and altered leaf color (Liu *et al*. 2013). The impact of these proteins on seedling development was first observed in maize (*Zea mays* L.), where the *Hcf60* mutation that affects the plastid ribosome small subunit protein PRPS17 significantly reduces photosynthesis and plastid translation levels, resulting in light-green seedlings (Schultes *et al*. 2000). *PRPL1* is essential for *Arabidopsis* embryo development. T-DNA knockout of *PRPL1* results in embryonic lethality, primarily attributed to disrupted fatty acid biosynthesis —a critical process for maintaining membrane integrity, signaling, and enzymatic regulation (Romani *et al*. 2012). This lethality stems from disrupted chloroplast translation of *accD*, which encodes the β subunit of heteromeric acetyl-CoA carboxylase (ACCase), the key enzyme converting acetyl-CoA to malonyl-CoA (Bryant *et al*. 2011).

In a recent study, we identified a Chinese cabbage mutant, *Mut298*, through ethyl methanesulfonate (EMS) mutagenesis (Lu *et al*. 2016; Sun *et al*. 2022). Unlike the wild type, *Mut298* exhibits golden yellow leaves across the entire plant and shows retarded growth. Genetic analysis indicated that a single recessive mutation controls this leaf yellowing trait. The candidate gene responsible for the yellowing of Chinese cabbage leaves, *BrPRPL1*, was pinpointed using genome sequencing of bulked DNA (MutMap) and kompetitive allele-specific PCR (KASP). This gene encodes the chloroplast ribosomal large subunit protein L1. In the mutant line *Mut298*, a single nucleotide substitution from C to T change glycine to arginine in the seventh exon of *BrPRPL1*. This specific alteration in Chinese cabbage leads to a dysfunctional ribosomal translation system. This dysfunction impairs chloroplast development, resulting in leaf yellowing and stunted growth. Identifying *Mut298* has revealed critical sites affecting *BrPRPL1* function in chloroplast development, offering valuable resources for Chinese cabbage breeding. Moreover, this study elucidates the effects of *PRPL1* mutation on chloroplast ribosome translation and establishes a framework for investigating *PRPL1*'s regulatory functions in plant growth and development. Currently, no studies have reported *PRPL1*'s involvement in regulating leaf color development in plants. Thus, our findings not only advance the understanding of *PRPL1*'s regulatory mechanisms in leaf color but also provide both theoretical foundations and genetic resources for breeding Chinese cabbage varieties with diverse leaf coloration.

2. Materials and methods

2.1. Experimental materials and cultivation conditions

We used the Chinese cabbage inbred line 'A03' (wild type, WT) and the leaf yellowing mutant *Mut298*, derived from EMS mutagenesis of WT, as experimental materials. The M_5 homozygous mutant of *Mut298* was established after multiple generations of self-pollination. We performed crosses between *Mut298* and WT to produce F_1 and F_2 progeny. In August 2023, seeds were sown in a greenhouse at Hebei Agricultural University: 10 F_1, 30 WT, 30 *Mut298*, and 270 F_2 seeds. The physiological indicators of the fourth leaf, counted from inside to outside during the rosette stage (40 days after sowing), were measured. Samples were immediately frozen in liquid

nitrogen and stored at -80℃ for subsequent DNA, RNA, and protein analyses.

2.2. Genetic analysis of mutant phenotypes

Phenotypic evaluations were conducted for WT, *Mut298*, F_1, and F_2 plants. The segregation ratios for F_1 were calculated, and the F_2 ratios were analyzed using a chi-square test to determine Mendelian inheritance.

2.3. Determination of physiological parameters

On the harvest day (14 days after sowing), the fresh weights of shoots and roots were measured. Subsequently, the samples were oven-dried at 180°C for 72 h to determine their dry weights. Twenty replicates were performed for each treatment. The total leaf area was assessed using LI-3100C (LI-COR Inc. , Lincoln, USA). Leaf dry mass per area (LMA) was computed by dividing the leaf dry weight by the leaf area. Twenty replicates were conducted for each treatment. The superoxide anion and hydrogen peroxide contents in Chinese cabbage were determined using a plant superoxide anion staining kit (Servicebio Inc., Wuhan, China) and a plant hydrogen peroxide staining kit (Servicebio Inc., Wuhan, China), respectively. Chinese cabbage was grown in vermiculite for five days to measure root length, with thirty replicates per treatment.

Chlorophyll was extracted using the ethanol-acetone method (Liu et al. 2022). Specifically, we precisely weighed 0.2 g of fresh leaves and placed them into 50 ml centrifuge tubes, adding 10 ml of a 1:1 ($v•v^{-1}$) ethanol-acetone solution. The leaves were extracted in darkness for 24 hours until completely decolorized. Absorbance at 646 nm and 663 nm was measured using UV-1800 (Shimadzu Inc., Kyoto, Japan). Chlorophyll content was calculated using the following formulas:

Chlorophyll a ($mg•g^{-1}$) = (12.21 A663 - 2.81 A646) V•1000W^{-1}

Chlorophyll b ($mg•g^{-1}$) = (20.13 A646 - 5.03 A663) V•1000W^{-1}

Where V is the volume of the extraction solution in ml and W is the leaf weight in g.

Net photosynthesis rate measurements were conducted between 9:00-11:00 on a clear day AM using LI-6800 (LI-COR Inc., Nebraska, USA) on the fourth true leaf from the inside out. For WT and *Mut298*, three seedlings (15 days after sowing) with consistent growth were selected, and PlantExplorer^{Pro+} (PhenoVation Inc., Wageningen, Netherlands) was used to measure chlorophyll fluorescence parameters in these seedlings.

2.4. Observation of chloroplast ultrastructure

The leaves of WT and *Mut298* were fixed and examined following the protocol described by Woodson *et al* (2015). Ultrathin sections were prepared using a diamond knife on a Leica EM UC7 ultramicrotome (Leica Microsystems Inc., Buffalo Grove, USA). Chloroplasts were observed and photographed using a H7600 transmission electron microscope (Hitachi Inc., Tokyo, Japan).

2.5. Identification of the candidate gene through MutMap and KASP

DNA was extracted from 30 F_2 plants exhibiting the mutant phenotype and 30 F_2 plants with the WT phenotype using the CTAB method. Equal quantities of DNA from each phenotype group were pooled to create separate mutant and WT pools. These pools were then sequenced on an Illumina HiSeq 2500 platform (KeyLab Bio Inc., Guangzhou, China). The raw data were filtered to obtain high-quality reads, which were aligned with the V2.5 Chinese cabbage reference genome available at BrassicaDB (http://brassicadb.cn). SNP analysis was conducted, and candidate loci were screened with an SNP index ≥ 0.8.

DNA was extracted from three *Mut298* plants, three WT plants, five F_2 plants with the mutant phenotype, and

five F_2 plants with the WT phenotype. This was followed by sequencing analysis to exclude mutant genes that did not conform to the expected genotype-phenotype correlations. The primers for sequencing are presented in Appendix J. KASP was then used to identify the candidate gene among the remaining mutant genes.

2.6. Transcriptome analysis

Total RNA was extracted from the leaves at the same position from both WT and *Mut298* seedlings using TRIzol reagent (Thermo Fisher Scientific Inc., Waltham, USA). mRNA containing PolyA was isolated from the total RNA and subsequently fragmented under 94°C. cDNA synthesis was performed using SuperScript™ II Reverse Transcriptase (Invitrogen Inc., Carlsbad, USA) from the fragmented RNA. Second-stranded DNAs labeled with uracil were synthesized using DNA Polymerase I and RNase H (NEB Inc., Ipswich, USA). The uracil-labeled (U-labeled) DNAs were then treated with UDG enzyme (NEB Inc., Ipswich, USA) to prepare for cDNA library construction. A cDNA library of approximately 300 ± 50 bp was generated through PCR amplification. Sequencing was conducted using the Illumina NovaSeq 6000 system (LC-Bio Technology Inc., Hangzhou, China), producing 2x150 bp paired-end reads. Final sequencing was conducted using the Illumina NovaSeq 6000 system (LC-Bio Technology Inc., Hangzhou, China), which performed 2×150 bp paired-end sequencing.

2.7. Virus-induced gene silencing (VIGS) of the candidate gene *BrPRPL1*

Functional validation of the candidate gene *BrPRPL1* was carried out using a TYMV-induced gene silencing method tailored for the *Brassicaceae* family (Hou *et al*. 2018). The VIGS vector was engineered by a biological company (GeneScript Inc., Nanjing, China). Plasmids with a high concentration (1567 ng•μL^{-1}) were prepared for the experiment. When WT plants developed two true leaves, they were selected for VIGS treatment. After observing phenotypic changes—the transition of leaf color from green to yellow in pTY-*BrPRPL1* plants—the plants were photographed and sampled. Quantitative RT-PCR (qRT-PCR) was employed to assess the silencing efficiency of *BrPRPL1*.

2.8. Western blot of chloroplast ribosome-encoded proteins

Leaves of WT, *Mut298* and pTY-*BrPRPL1* were rapidly ground into a fine powder in liquid nitrogen and transferred to 2 mL centrifuge tubes. Each tube received 800 μL of protein lysis buffer (Beyotime Inc., Shanghai, China), followed by centrifugation at 12,000 rpm for 5 minutes. The supernatant was collected, and protein concentration was measured. The samples were then heated at 95°C for 10 minutes before loading 20 μg onto SDS-PAGE for electrophoresis to separate proteins.

Following SDS-PAGE, the proteins were transferred onto a polyvinylidene difluoride (PVDF) membrane (Beyotime Inc., Shanghai, China). The membrane was blocked in a blocking solution for 1 hour at room temperature, then incubated with specific primary antibodies targeting actin at a dilution of 1:5000 v•v^{-1} (AT0004, Engibody Inc., Milwaukee, USA), RbcL at 1:2000 (v•v^{-1}) (A01110, Abbkine Inc., Wuhan, China), PsaB at 1:5000 (v•v^{-1}) (PHY0054A, PhytoAB Inc., California, USA), PsaA at 1:2000 (v•v^{-1}) (PHY0368A, PhytoAB Inc., California, USA), and PetB b6/f at 1:2000 (v•v^{-1}) (PHY0020S, PhytoAB Inc., California, USA). The secondary antibodies used were specific to mouse (BF03001X, Biodragon Inc., Suzhou, China) and rabbit (BA01235136, Bioss Inc., Beijing, China). Protein signals were detected using the Odyssey Infrared Imaging System (LI-COR Biosciences Inc., Lincoln, USA).

2.9. qRT-PCR analysis and subcellular localization

Total RNA was extracted from leaves at the same position from both WT and *Mut298* plants during the seedling stage and rosette stage, as well as from samples for transcriptome analysis using a total RNA extraction kit (Tiangen Inc., Beijing, China). Each sample included three biological replicates for both WT and *Mut298*, with three technical replicates for each biological replicate. Reverse transcription to synthesize first-strand cDNA for qRT-PCR was performed using a kit (Vazyme Inc., Nanjing, China). The ChamQ Universal SYBR qPCR Master Mix (Vazyme Inc., Nanjing, China) was utilized for qRT-PCR on a QuantStudio 5 system (Thermo Fisher Scientific Inc., Waltham, USA) under the following thermal cycling conditions: initial denaturation at 95℃ for 2 minutes, followed by 40 cycles of 10 sec at 95℃, 30 sec at 60℃, and a final melt curve stage of 15 sec at 95℃, 1 minute at 60℃, and 15 sec at 95℃. The relative expression levels of genes were quantified using the $2^{-\triangle\triangle Ct}$ method. Gene-specific primers for qRT-PCR are presented in Appendix J.

Protoplasts were extracted from Chinese cabbage and transformed according to Yu's method (Yu et al., 2024). The CDS sequence of *BrPRPL1* was cloned into the pMD18-T vector. The plasmid was then transformed into Chinese cabbage protoplasts using the PEG-mediated protoplast transfection method (Yu et al., 2024). GFP fluorescence signals were observed using a LSM900 (Zeiss Inc., Oberkochen, Germany). The primers for subcellular localization are presented in Appendix J.

2.10 Statistical analysis

SPSS Statistics 21.0 and Origin 2019 were used for data analysis and visualization, respectively. Physiological and qRT-PCR data were analyzed using Tukey's new multiple range test at $p \leq 0.05$ or *t*-test at $p \leq 0.05$.

3. Results

3.1. Morphology and chloroplast structure of WT and *Mut298*

Throughout the seedling and rosette stages, *Mut298* exhibited leaf yellowing and reduced growth rate compared to WT (Figs. 1A and B). Transmission electron microscopy (TEM) revealed that chloroplasts in WT were ellipsoidal, well-developed, and neatly arranged with normally stacked granal lamellae, starch grains and thylakoid grana (Fig. 1C). In contrast, chloroplasts in *Mut298* were disorganized, less compact, displayed diminished starch grain accumulation and indistinct thylakoid grana (Fig. 1D). This indicated that the yellowing of the *Mut298* leaves is related to abnormal chloroplast development.

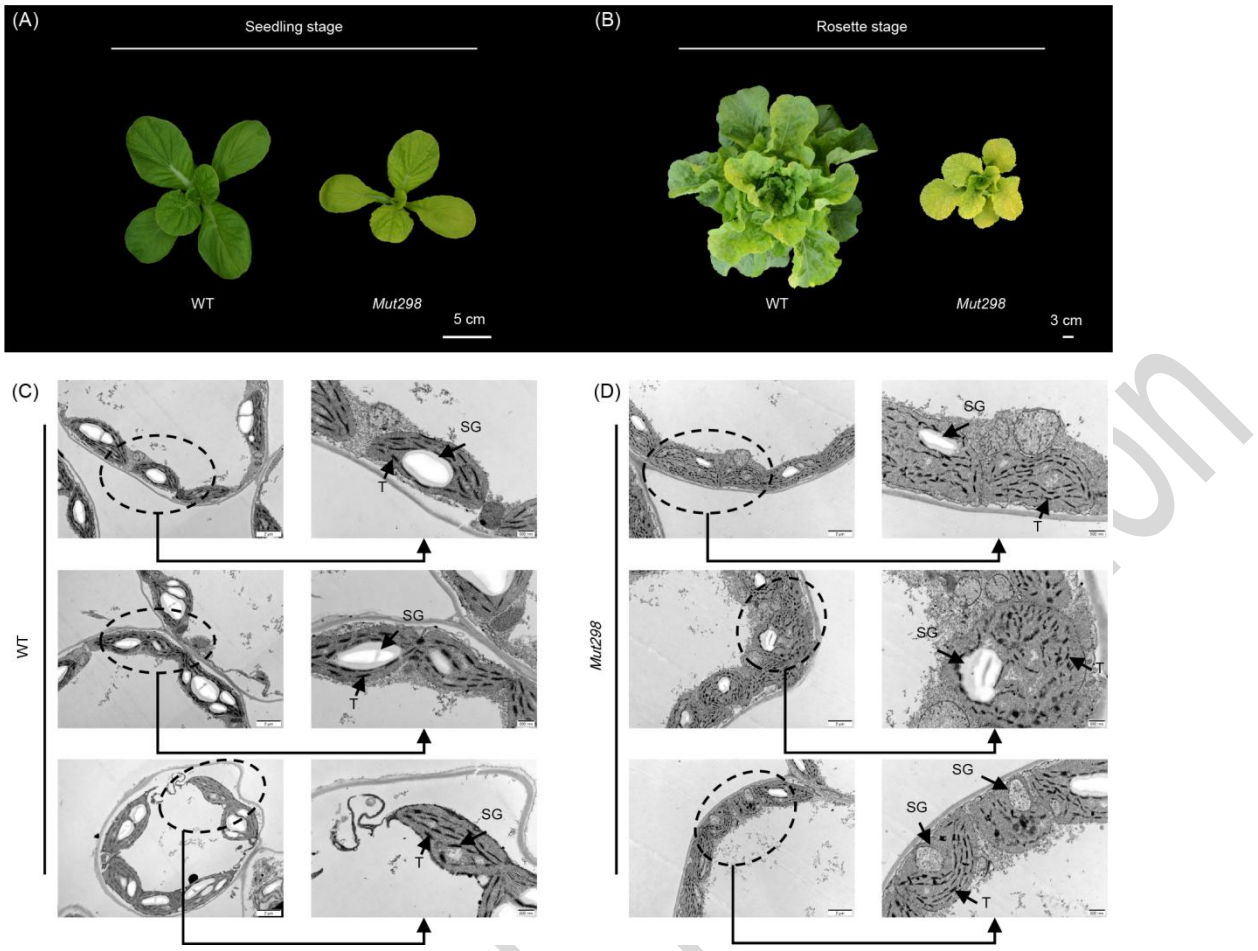

Fig. 1 Physiological indices of WT and *Mut298*. A, phenotypes of WT and *Mut298* plants at the seedling stage. Scale bar, 5 cm. B, phenotypes of WT and *Mut298* plants at the rosette stage. Scale bar, 3 cm. C, ultrastructure of chloroplasts in WT. T, thylakoid grana; SG, starch granule. D, ultrastructure of chloroplasts in *Mut298*. WT represents wild type of Chinese cabbage.

3.2. Physiological parameters of WT and *Mut298*

The shoot fresh weight and shoot dry weight of WT were significantly higher than those in *Mut298* (Table 1). However, the root length of WT was significantly lower than that in *Mut298* (Table 1 and Appendix E). There was no significant difference between the imaging of superoxide anion and hydrogen peroxide (Appendix F). The yellowing of the *Mut298* leaves resulted in a significant reduction in chlorophyll content and photosynthetic parameters compared to the WT. Chlorophyll a, chlorophyll b content and net photosynthetic rate were significantly lower by 1.5, 1.7- and 0.5-fold, respectively, in *Mut298* than in WT (Figs. 2A, B and D). Chlorophyll fluorescence imaging revealed distinct differences between the WT and the *Mut298* mutant in terms of chlorophyll content and fluorescence parameters, including maximal quantum yield of PSII (Fv/Fm), photochemical efficiency of PSII in the light (Fq'/Fm') and relative electron transport rate (rETR). Specifically, the imaging color of chlorophyll for WT was yellow, in contrast to the blue color observed for *Mut298* (Appendix C), indicating lower chlorophyll content in *Mut298* (Appendix C). Fluorescence imaging for Fv/Fm and Fq'/Fm' in *Mut298* showed red, whereas WT displayed yellow (Figs. 2F and G), suggesting reduced Fv/Fm and Fq'/Fm' values in *Mut298* (Figs. 2J and K). Additionally, the rETR imaging showed *Mut298* in blue and the WT in red (Appendix C), indicating a lower rETR in *Mut298* (Appendix C).

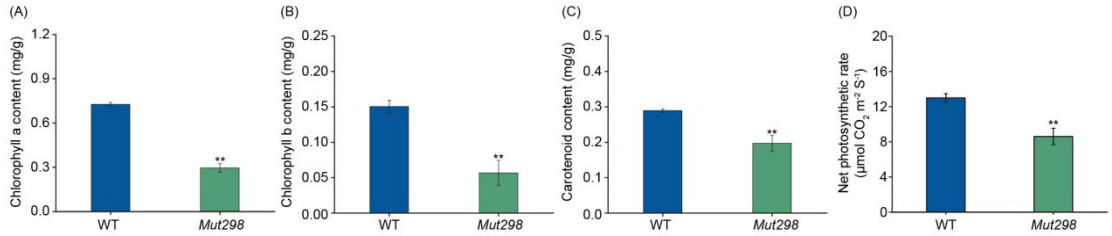

Fig. 2 Pigment content and photosynthetic parameters. A-D, levels of chlorophyll a, chlorophyll b, carotenoid and net photosynthetic rate in WT and *Mut298*. Error bars represent standard deviation (SD; n = 3). *** indicates significant differences at $p < 0.01$ based on the Student's *t*-test.

Table 1. Growth parameters of WT and *Mut298*

Growth parameters / Sample	SFW	RFW	SDW	RDW	RL	LA	LN	LWC	LMA
WT	4.328 ± 0.970[a]	0.156 ± 0.072[a]	0.388 ± 0.126[a]	0.011 ± 0.002[a]	4.717 ± 0.288[a]	22.177 ± 4.583[a]	7.000 ± 0.725[a]	0.91 ± 0.018[a]	17.824 ± 5.724[a]
Mut298	2.651 ± 0.521[b]	0.132 ± 0.059[a]	0.133 ± 0.034[b]	0.006 ± 0.001[b]	7.263 ± 0.593[b]	21.337 ± 4.911[a]	6.000 ± 0.459[b]	0.95 ± 0.010[a]	6.285 ± 1.288[b]

Twenty replicates were conducted for SFW, RFW, SDW, RDW, RL, LA, LN, LWC and LMA. The different letters in each column indicate significant differences between WT and *Mut298* at $p < 0.05$, determined by *t*-test. SFW, RFW, SDW, RDW, RL, LA, LN, LWC and LMA represent shoot fresh weight, root fresh weight, shoot dry weight, root dry weight, root length, leaf area, leaf number, leaf water content and leaf mass per area. WT represents wild type of Chinese cabbage.

3.3. Changes in chloroplast protein homeostasis and retrograde signaling

To explore the changes in gene expression levels related to metabolic pathways in WT and *Mut298*, seedling leaves were sampled for transcriptome analysis. The results showed that a total of 4863 differentially expressed genes (DEGs) between the two genotypes (Appendix A). GO enrichment analysis revealed that these DEGs are primarily enriched in biological processes associated with DNA transcription (Appendix B). KEGG enrichment analysis revealed that the DEGs are mainly enriched in pathways related to the plant hormone signal transduction (Appendix B). For the chloroplast retrograde signaling and chloroplast proteolysis that we are concerned with. There was a total of 25 DEGs associated with chloroplast retrograde signaling (Appendix K). Among them, eight DEGs were significantly downregulated and seventeen DEGs were significantly upregulated (Figs. 3A and B; Appendix K). All six DEGs (*EGY2*, *NANA*, *PreP1*, *FtsH6*, *FtsH11*, and *FtsH12*) related to chloroplast proteolysis were significantly upregulated (Fig. 3C; Appendix L). A large number of DEGs related to chlorophyll synthesis (Fig. 3D; Appendix M) and photosynthesis were upregulated (Fig. 3E; Appendix N). The expression levels of nine genes (*CHLI1*, *CHLM*, *LHCA3*, *PRIN2*, *SG1*, *PAP6*, *NANA*, *FtsH11* and *FLU*) were significantly higher in *Mut298* than those in WT (Appendix G), which was consistent with the transcriptional level of transcriptome.

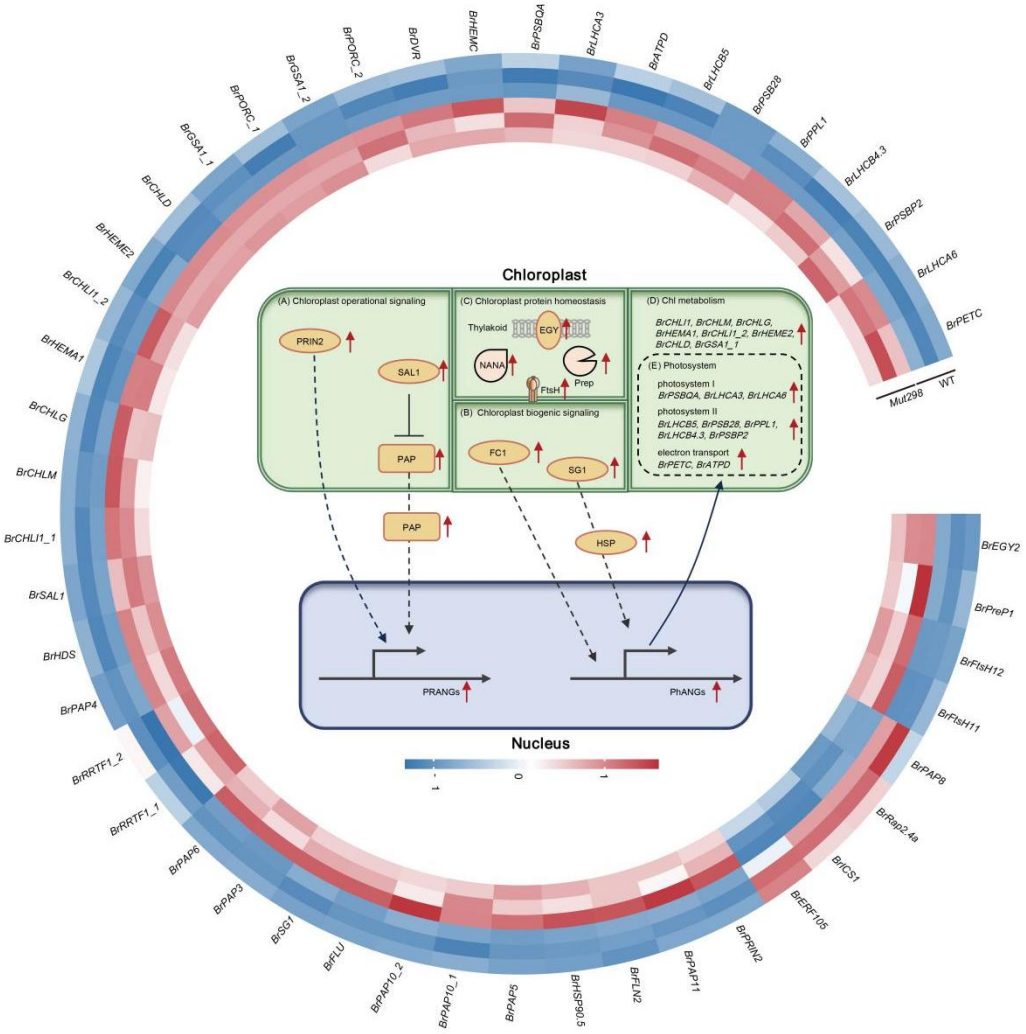

Fig. 3 The DEGs in chloroplast protein homeostasis and retrograde signaling. A, retrograde signaling by mature chloroplasts. B, retrograde signaling by developing chloroplasts. C, proteolytic genes in chloroplast protein homeostasis. D, chlorophyll metabolism related genes. E, photosynthesis related genes. Genes regulated by retrograde signals include photosynthesis-associated nuclear genes (PhANGs) and plastid redox–associated nuclear genes (PRANGs). The DEGs are visualized by heat map. The red font represents up-regulated genes, and blue font represents down-regulated genes. The red arrow represents up-regulated genes.

3.4. Genetic analysis of mutant traits and identification of the candidate gene

Genetic analysis revealed that all *Mut298* × WT F_1 plants obtained exhibited the WT phenotype, indicating that the causal mutation in *Mut298* is recessive. In addition, 202 and 68 of *Mut298* × WT F_2 progeny exhibited the WT and mutant phenotype, respectively and a chi-square test confirmed a 3:1 segregation ratio, typical of a single recessive gene affecting these traits (Table 2).

The candidate region was pinpointed on chromosome 4 via MutMap analysis (Fig. 4A). Utilizing a ΔSNP index greater than 0.8 as the screening criterion, two non-synonymous mutation sites (*BAA04g00040* and *BAA04g02470*) were identified, each featuring a single nucleotide substitution from C to T (Table 3). PCR sequencing revealed that the genotype-phenotype correlation for *BAA04g02470* was inconsistent, leading to its preliminary exclusion from further analysis (Appendix I). Subsequently, KASP analysis on *BAA04g00040* (*BrPRPL1*) confirmed a complete concordance between genotype and phenotype in the F_2 population (Figs. 4 B-D). In the mutant line *Mut298*, a single nucleotide substitution from C to T change glycine to arginine in the domain of *BrPRPL1* (Fig. 4E; Fig. 4F).

Fig. 4 *BrPRPL1* is the candidate gene. A, identification of genomic regions containing causal mutations for *Mut298* using MutMap. SNP index plots for *Mut298* span all 10 chromosomes, with individual symbols representing SNPs. The x-axis indicates chromosomal positions, and the mean SNP index value is depicted by a black line through sliding window analysis. SNPs on chromosome A04 represent the predicted causal mutations for *Mut298*. B-D, KASP genotyping assay for *BrPRPL1* in an F_2 population. Displays include 105 individuals on the left (F_2), 105 in the middle (F_2), and 60 on the right (3 WT, 3 *Mut298*, and 54 F_2). Blue, green, and red represent WT, heterozygous, and mutant (*Mut298*) genotypes, respectively. FAM, 6-carboxy-fluorescein; HEX, hexachlorofluorescein. E, structural diagram of *BrPRPL1* and the mutation site. The blue squares represent exons, the blue lines represent introns, and the red arrow indicates a single nucleotide substitution from C to T at 1702 bp. F, structural diagram of BrPRPL1. The blue square represents

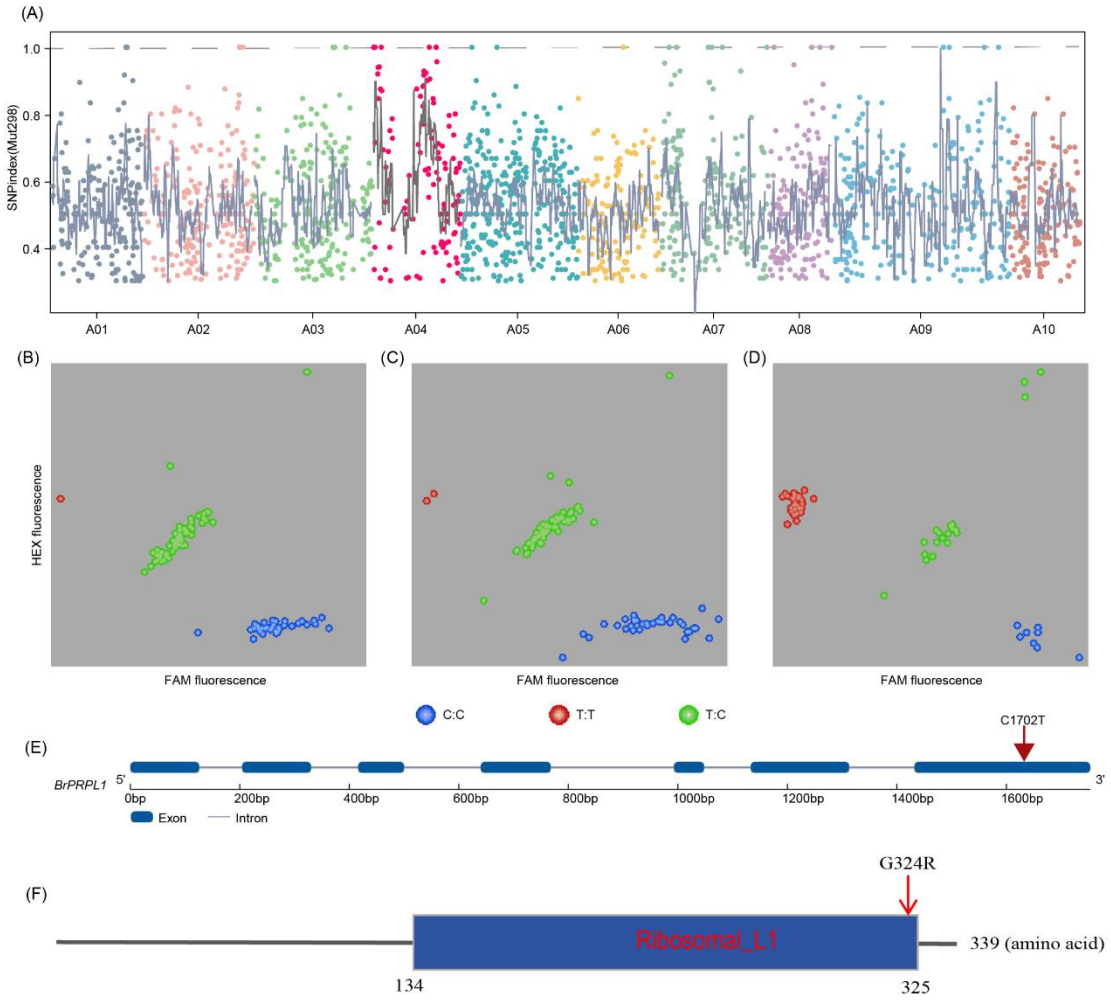

the domain of BrPRPL1 (Ribosomal_L1). The red arrows indicate the mutated amino acid. G and R represent glycine and arginine, respectively.

Table 2. Segregation ratios of F_1 and F_2 between WT and *Mut298* plants

Generation	Plants (WT phenotype)	Plants (*Mut298* phenotype)	Total plants	Segregation ratio	χ^2
F_1	10	0	10	10:0	
F_2	202	68	270	2.97:1	0.00

WT represents wild type of Chinese cabbage.

Table 3. Candidate genes obtained through MutMap.

Gene ID	Chromosome	Structure type	Position	Wild type site	Mutant site	SNP-index
BAA04g00040	A04	exonic (nonsynonymous)	16284	C	T	1.00
BAA04g02470	A04	exonic (nonsynonymous)	1466890	C	T	0.92

MutMap represents genome sequencing of bulked DNA

3.5. *BrPRPL1* silencing results in leaf yellowing of Chinese cabbage

Next, we employed the Virus-Induced Gene Silencing (VIGS) technique to investigate the function of *BrPRPL1* in Chinese cabbage using the pTY vector. Plants silenced for the phytoene desaturase (*PDS*) gene displayed a bleached phenotype (Fig. 5A), confirming the effective delivery and functionality of the VIGS system in disrupting gene expression. qRT-PCR analysis confirmed that the silencing efficiency of *BrPRPL1* in pTY-*BrPRPL1* plants was 96%, 95%, and 88%, respectively, indicate the successful silencing of *BrPRPL1* (Fig. 5B). Silencing of the candidate gene *BrPRPL1* resulted in leaf yellowing, whereas plants transformed with the pTY empty vector control remained (Fig. 5A). Additionally, compared with PDS and pYT, pTY-*BrPRPL1* exhibited different colors in images generated from chlorophyll and chlorophyll fluorescence parameters (Fv/Fm, Fq'/Fm', and rETR). The imaging color of chlorophyll for PDS and pTY-*BrPRPL1* was blue, in contrast to the yellow color observed for pTY (Appendix D), indicating that chlorophyll contents in these two lines were lower than that in pTY (Appendix D). Consistent with this observation, chlorophyll a and chlorophyll b content in the pTY-*BrPRPL1* and PDS plants was indeed significantly lower by 1.2- and 9.1-fold and 1.9- and 5.3-fold, respectively, than in the pTY plants (Figs. 5C and D). Moreover, the imaging colors of Fv/Fm and Fq'/Fm' for PDS and pTY-*BrPRPL1* were red, whereas those for pTY were yellow (Figs. 5F and G), suggesting that the Fv/Fm and Fq'/Fm' values in PDS and pTY-*BrPRPL1* were lower than in pTY (Figs. 5J and K). The imaging color of the rETR for PDS and pTY-*BrPRPL1* was blue, in contrast to the red color observed for pTY (Appendix D), indicating that rETR is lower in PDS and pTY-*BrPRPL1* than in pTY (Appendix D). These results indicated that *BrPRPL1* regulates leaf color development in Chinese cabbage.

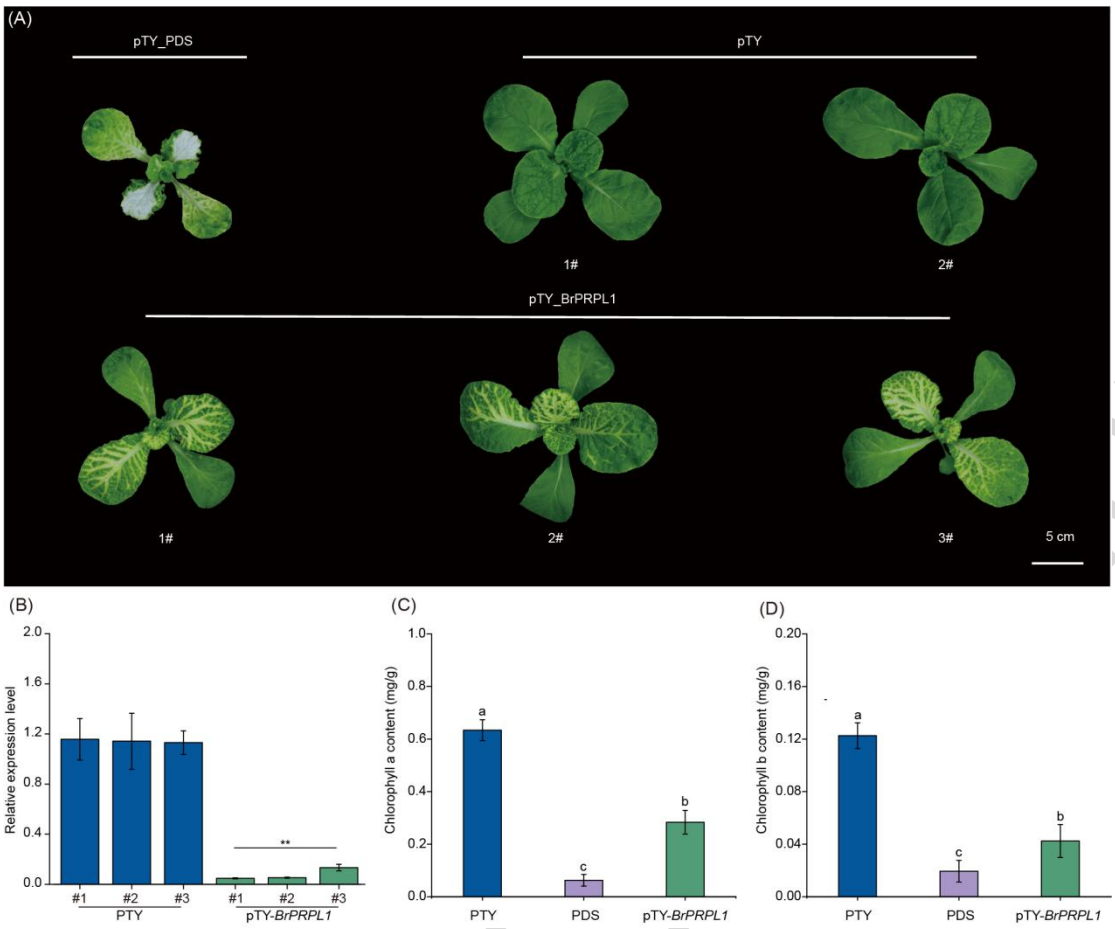

Fig. 5 Phenotypic and physiological indices of WT and *Mut298* after *BrPRPL1* silencing. A, phenotype of PDS, pTY, and pTY-*BrPRPL1* plants. Bar represents 5 cm. B, relative expression level of *BrPRPL1* in pTY-PRPL1 and pTY plants; error bars indicate SD (n = 3). Asterisks (***) denote significant differences at $p < 0.01$ based on Student's *t*-test. C-D, chlorophyll a and chlorophyll b content in pTY-*BrPRPL1*, pTY, and PDS plants; error bars represent SD (n = 3). Letters (a, b, c) indicate significant differences as determined by Tukey's new multiple range test at $p < 0.05$.

3.6. BrPRPL1 localizes to the chloroplast and affects the expression of several key ribosome-encoded proteins

The expression levels of *BrPRPL1* between *Mut298* and WT plants showed no significant difference at the seedling stage and rosette stage (Fig. 6B). The target gene *BrPRPL1* and its mutant form *mBrPRPL1* was separately expressed in frame with a GFP tag the pMD18-T vector in Chinese cabbage protoplasts to investigate its subcellular localization. We observed that the GFP fluorescence coincided with chlorophyll autofluorescence (Fig. 6A), confirming the localization of *BrPRPL1* and *mBrPRPL1* within the chloroplasts.

A single nucleotide change from C to T in *BrPRPL1* significantly reduces the expression of chloroplast genome-encoded proteins. Western blot analysis revealed that the RbcL protein, encoded by the chloroplast ribosome and a component of Rubisco's large subunit, was expressed at significantly lower levels in *Mut298* plants compared to WT plants (Fig. 6C). Moreover, the critical PSI proteins PsaA and PsaB were nearly absent in *Mut298* plants but expressed normally in WT plants (Fig. 6C). These findings support a role of *BrPRPL1* in influencing the stability or expression of these key photosynthetic proteins. The expression level of RbcL, PsaA and PsaB in

pTY-*BrPRPL1* was consistent with the *Mut298* (Appendix H).

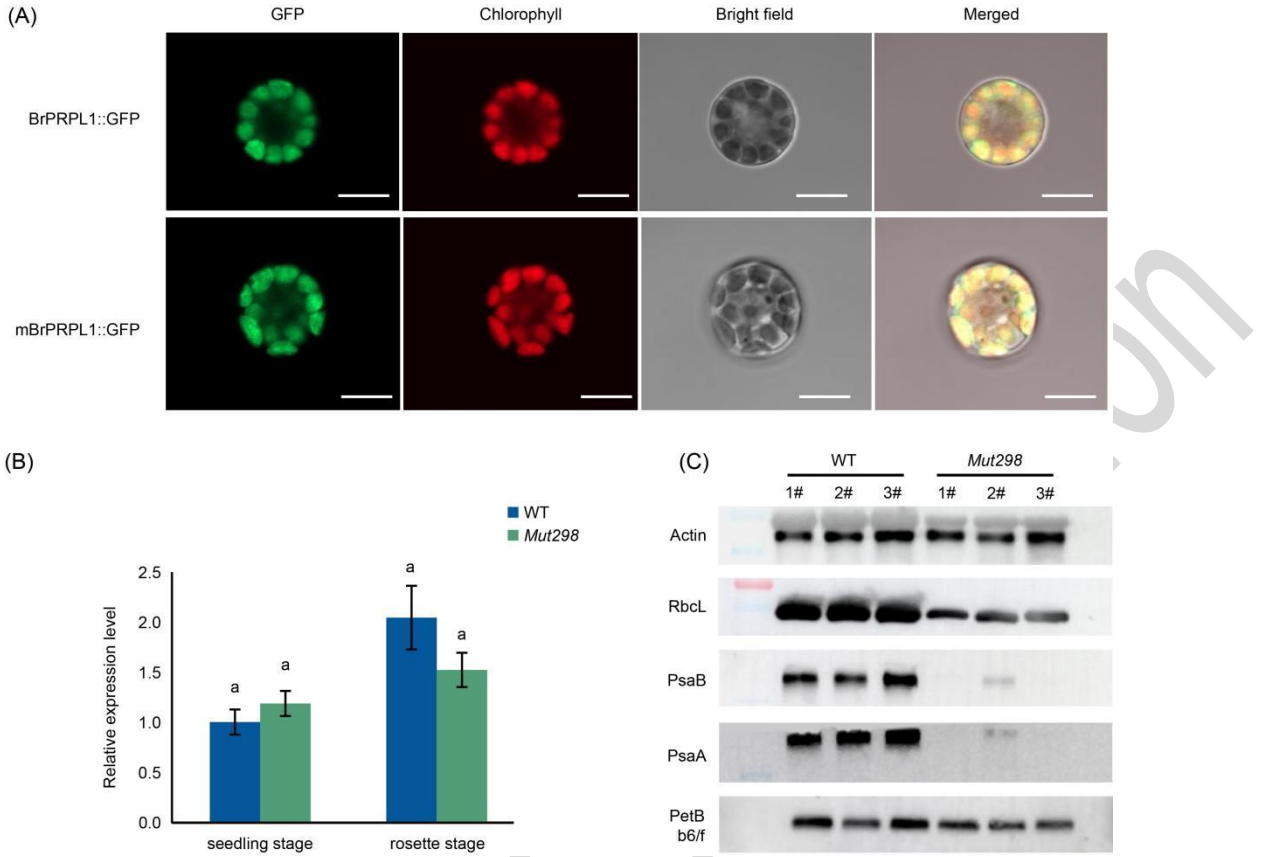

Fig. 6 Subcellular localization of BrPRPL1 and mBrPRPL1 and western blot analysis of chloroplast encoded proteins. A, subcellular localization of BrPRPL1 and mutant mBrPRPL1. Images display GFP (green), chlorophyll autofluorescence (red), bright field, and merged views. Scale bar = 10 μm. B, relative expression levels of *BrPRPL1* at the seedling stage and rosette stage in WT and *Mut298* plants; error bars represent SD (n = 3). Same letters indicate no significant differences according to Student's *t*-test. C, expression levels of Actin, RbcL, PsaB, PsaA, and PetB b6/f in WT and *Mut298* plants. There are three biological replicates of WT and *Mut298*.

4. Discussion

4.1. The *BrPRPL1* mutation disrupts chloroplast ribosome translation and causes abnormal chloroplast development and leaf yellowing

In a recent study, we identified a leaf yellowing mutant of Chinese cabbage, *Mut298*, through EMS mutagenesis (Lu *et al*. 2016; Sun *et al*. 2022). The candidate gene for *Mut298* was identified as *BrPRPL1* using MutMap and KASP (Figs. 4A-E). The silencing of *BrPRPL1* in Chinese cabbage led to significantly reduced *BrPRPL1* expression (Fig. 5B), causing a notable yellowing phenotype (Fig. 5A) as well as reduced chlorophyll content, and chlorophyll fluorescence parameters (Figs. 5C-L), mirroring those seen in *Mut298* plants (Figs. 1A and B; Appendix C). These results confirm the role of *BrPRPL1* in regulating leaf yellowing in Chinese cabbage.

Rubisco is a key enzyme in photosynthesis, responsible for catalyzing the first step of carbon dioxide fixation

(Cocon and Luis 2024). Here, the *BrPRPL1* mutation in Chinese cabbage disrupts ribosomal translation, markedly decreasing the levels of RbcL—the large subunit of Rubisco encoded by the chloroplast DNA (Wang *et al*. 2023), PsaA and PsaB proteins, which are core proteins of photosystem I (PSI), in *Mut298* (Fig. 6C), indicating severe disruption of chloroplast ribosome translation. Consistent with this result, a previous study reported that a mutation in the 50S large subunit protein of the chloroplast ribosome, encoded by the *PRPL11* gene, significantly reduces the translation rate of *RbcL*, leading to substantial reductions in the level of the PSI subunits and components of the PSII core complex (D1, D2, CP43, and CP47) as well as the α and β subunits of the ATPase complex in *Arabidopsis*, leading to a similar pale green leaf and slow growth phenotype (Pesaresi *et al*. 2001). Mutations in other chloroplast ribosomal proteins can also impair ribosome translation, thereby affecting plant growth and development. The mutation of *SVR8*, which encodes the L24 protein component of the chloroplast ribosome's large subunit in *Arabidopsis*, has been found to cause specific defects in chloroplast rRNA processing (Liu *et al*. 2013). Mutation of the plastid ribosomal protein S5 (RPS5) results in a dramatic decrease in chloroplast 16S rRNA abundance and severely impairs 16S rRNA processing, thereby affecting ribosome function and plastid translation (Zhang *et al*., 2016). These molecular defects manifest visibly as alterations in leaf color.

The *BrPRPL1* mutation identified in this research leads to chloroplast structural abnormalities (Figs. 1C and D), which, in turn, significantly reduce chlorophyll synthesis (Figs. 2A and B). In other plant species, mutations in chloroplast ribosomal proteins also alter pigment content and photosynthetic efficiency, thereby impairing plant growth and development. The *Hcf60* mutation, which disrupts small subunit protein PRPS17, significantly reduces both photosynthetic and chloroplast translation capacities, leading to light-green seedlings in maize (Schultes *et al*. 2000). In rice, the *ASL2* mutation, which encodes the chloroplast 50S ribosomal large subunit protein L21, leads to reduced chlorophyll content and abnormal chloroplast development, producing albino seedlings (Lin *et al*. 2015). Similarly, T-DNA knockout of *prpl13* in rice significantly alters the expression levels of photosynthesis- and chloroplast development-related genes, drastically reducing chlorophyll and carotenoid content and resulting in an albino phenotype (Lee *et al*. 2019). Chlorophyll a and chlorophyll b are crucial for photosynthesis, as these molecules absorb light energy and facilitate electron transfer (Shimoda *et al*. 2012). Specifically, chlorophyll a is essential for photochemistry, while chlorophyll b is necessary for stabilizing the main light-harvesting chlorophyll-binding protein (Tanaka and Tanaka 2011). Consistent observations of decreased net photosynthetic efficiency and altered chlorophyll fluorescence parameters in *Mut298* (Figs. 2D-L) underscore the pivotal role of *BrPRPL1* in maintaining chloroplast function and overall plant health. The mutation in *BrPRPL1*, a gene regulating yellow-leaf in Chinese cabbage, provides a potential target for marker-assisted breeding. By developing functional molecular markers upon identification of the mutation site sequence, early and precise selection of the yellow-leaf trait can be achieved. This marker system enhances breeding efficiency for specific objectives including backcross breeding and gene pyramiding, with particular application value for developing stress-tolerant/ornamental varieties. When this gene's editability is confirmed, the associated markers may further serve as screening tools for CRISPR-edited progenies, thereby advancing precision breeding in Chinese cabbage.

4.2. A point mutation in *BrPRPL1* does not lead to embryonic lethality in Chinese cabbage

PRPL1 is essential for embryo development and the T-DNA knockout of *PRPL1* leads to embryonic lethality in *Arabidopsis* (Romani *et al*. 2012). This lethality is linked to disruptions in essential metabolic pathways, notably

the biosynthesis of fatty acids. Fatty acids are crucial components of the cell membrane and play significant roles in signal transduction and the regulation of enzyme activity. Alterations in fatty acid biosynthesis can have serious consequences during embryogenesis. The chloroplast-localized heteromeric ACCase is central to this process by converting acetyl-CoA to malonyl-CoA. The chloroplast gene *accD* in *Arabidopsis* encodes the β subunit of ACCase. Disruption of chloroplast translation affects ACCase synthesis by impacting the translation of *accD* (Bryant *et al*. 2011). Additionally, the T-DNA knockout of the gene *CAC1A*, which encodes the biotin carboxyl-carrier protein of heteromeric ACCase, results in embryonic lethality, reinforcing the critical role of proper ACCase function during early plant development in *Arabidopsis* (Li *et al*. 2011).

Chinese cabbage and *Arabidopsis* each contains one copy of the *PRPL1* gene. While *PRPL1* mutations cause embryonic lethality in *Arabidopsis*, *BrPRPL1* mutations do not lead to such severe effects in Chinese cabbage. The absence of the plastid-encoded PRPS12 leads to an albino phenotype in maize, whereas lack of PRPS12 causes embryonic lethality in *Arabidopsis* (Asakura and Barkan 2006; Ostheimer *et al*. 2003). The discrepancy may be explained by the localization of *accD* transcription and translation. In maize, *accD* is encoded in the nucleus and translated in the cytoplasm, which allows embryonic development to proceed normally despite impaired chloroplast ribosome translation (Ostheimer *et al*. 2003; Asakura and Barkan 2006; Chalupska *et al*. 2008). This may also be the reason why embryo lethality does not occur in Chinese cabbage. The differential impacts of *PRPL1* mutations on embryonic development across species underscore the significant role of species-specific genetic and cellular contexts in determining the phenotypic outcomes of similar genetic alterations.

5. Conclusion

In this study, a golden-leaf mutant, *Mut298*, was obtained in Chinese cabbage through EMS mutagenesis. *BrPRPL1* was identified as the candidate gene regulating the yellowing leaf of Chinese cabbage. Silencing of *BrPRPL1* confirmed its involvement in regulating leaf color development of Chinese cabbage. Additionally, a single nucleotide change from C to T in *BrPRPL1* significantly reduces the expression of chloroplast genome-encoded proteins, such as RbcL, PsaA, and PsaB, and impaired chloroplast development, leading to golden yellow leaves in Chinese cabbage. To date, there have been no reports on the role of *PRPL1* in regulating leaf color development in plants. Therefore, this study enhances the understanding of the regulatory mechanisms of *PRPL1* in leaf color development and provides a theoretical foundation and genetic resources for breeding Chinese cabbage with diverse leaf colors.

Acknowledgements

This study was supported by the grants from the National Natural Science Foundation of China (32222076; 32330096; 32472736; 32272712), Hebei Natural Science Foundation (C2023204308, C2024204246), Central Guiding Local Technology Development Fund (246Z6312G, 246Z6311G), the Earmarked Fund for CARS (CARS-23), State Key Laboratory of North China Crop Improvement and Regulation (NCCIR2023ZZ-19).

Declaration of competing interest

The authors declare that they have no conflict of interest

Appendix associated with this paper is available on http://www.ChinaAgriSci.com/V2/En/appendix.htm

Appendices:

Appendix A. Volcano plots of differentially expressed genes (DEGs).

Appendix B. GO and KEGG enrichment analysis.

Appendix C. Chlorophyll fluorescence parameters of WT and *Mut298*.

Appendix D. Chlorophyll fluorescence parameters of WT and *Mut298* after *BrPRPL1* silencing.

Appendix E. Chinese cabbage seedlings grown in vermiculite for five days.

Appendix F. The imaging of superoxide anion and hydrogen peroxide.

Appendix G. The expression levels of nine DEGs by RT-qPCR analysis.

Appendix H. Expression levels of Actin, RbcL, PsaB, PsaA, and PetB b6/f in WT and pTY-*BrPRPL1*.

Appendix I. The genotype of WT, *Mut298* and F2.

Appendix J. Primers designed for qRT-PCR, subcellular localization and gene fragment sequencing.

Appendix K. DEGs related to chloroplast retrograde signaling.

Appendix L. DEGs related to chloroplast protein homeostasis.

Appendix M. DEGs related to chlorophyll synthesis.

Appendix N. DEGs related to photosynthesis.

References

Asakura Y, Barkan A. 2006. *Arabidopsis* orthologs of maize chloroplast splicing factors promote splicing of orthologous and species-specific group II introns. *Plant Physiology*, **142**, 1656-1663.

Bryant N, Lloyd J, Sweeney C, Myouga F, Meinke D. 2011. Identification of nuclear genes encoding chloroplast-localized proteins required for embryo development in *Arabidopsis*. *Plant Physiology*, **155**, 1678-1689.

Cazzonelli C I, Pogson B J. 2010. Source to sink: Regulation of carotenoid biosynthesis in plants. *Trends in Plant Science*, **15**, 266-274.

Chalupska D, Lee H Y, Faris J D, Evrard A, Chalhoub B, Haselkorn R, Gornicki P. 2008. *Acc* homoeoloci and the evolution of wheat genomes. *Proceedings of the National Academy of Sciences of the United States of America*, **105**, 9691-9696.

Cheng M Z, Meng F Y, Mo F L, Chen X L, Zhang H, Wang A X. 2022. Insights into the molecular basis of a yellow leaf color mutant (*ym*) in tomato (*Solanum lycopersicum*). *Scientia Horticulturae*, **293**, 110743.

Cocon K D, Luis P. 2024. The potential of rubisco in CO_2 capture and utilization. *Progress in Energy and Combustion Science*, **105**, 101184.

Fu Y T, Li X F, Fan B F, Zhu C, Chen Z X. 2022. Chloroplasts protein quality control and turnover: A multitude of mechanisms. *International Journal of Molecular Sciences*, **23**, 14.

Hou X, Zhang C, Gao L. 2018. A TYMV virus induced endogenous gene silencing method in *Brassicaceae* and its application. China, CN107557383A.

Kusumi K, Sakata C, Nakamura T, Kawasaki S, Yoshimura A, Iba K. 2011. A plastid protein NUS1 is essential for build-up of the genetic system for early chloroplast development under cold stress conditions. *Plant Journal*, **68**, 1039-1050.

Li X, Ilarslan H, Brachova L, Qian H R, Li L, Che P, Wurtele ES, Nikolau BJ. 2010. Reverse-genetic analysis of the two biotin-containing subunit genes of the heteromeric acetyl-coenzyme a carboxylase in *Arabidopsis*

indicates a unidirectional functional redundancy. *Plant Physiology*, **155**, 293-314.

Li J, Yu X, Cai Z. 2019. An overview of chlorophyll biosynthesis in higher plants. *Molecular Plant Breeding*, **29**, 639-636.

Linley P J, Landsberger M, Kohchi T. 2006. The molecular basis of heme oxygenase deficiency in the *pcd1* mutant of pea. *FEBS Journal*, **273**, 2594-2606.

Liu M Y, Ma W, Su X J, Zhang X M, Lu Y, Zhang S W, Yan J H, Feng D L, Ma L S, Taylor A, Ge Y J, Cheng Q, Xu K D, Wang Y H, Li N, Gu A X, Zhang J, Luo S X, Xuan S X, Chen X P, Scrutton N S, Li C W, Zhao J J, Shen S X. 2022. Mutation in a chlorophyll- binding motif of ferrochelatase enhances both heme and chlorophyll biosynthesis. *Cell Reports*, **41**, 10.

Liu X Y, Zheng M D, Wang R, Wang R J, An L J, Rodermel S R, Yu F. 2013. Genetic interactions reveal that specific defects of chloroplast translation are associated with the suppression of mediated leaf variegation. *Journal of Integrative Plant Biology*, **55**, 979-993.

Liu W K, Chen G L, He M M, Wu J Q, Wen W X, Gu Q S, Guo S R, Wang Y, Sun J. 2023. *ABI5* promotes heat stress-induced chlorophyll degradation by modulating the stability of *MYB44* in cucumber, *Horticulture Research*, **10**, uhad089.

Liu Z B, Mao L Z, Yang B Z, Cui Q Z, Dai Y H, Li X Q, Chen Y S, Dai X Z, Zou X X, Ou L J, Yang S. 2023. A multi-omics approach identifies *bHLH71*-like as a positive regulator of yellowing leaf pepper mutants exposed to high-intensity light. *Horticulture Research*, **10**, uhad098.

Lee J W, Jang S, Ryu S, Lee S, Park J, Lee S, An G. 2019. Mutation of plastid ribosomal protein L13 results in an albino seedling-lethal phenotype in rice. *Plant Breeding and Biotechnology*, 7, 395-404.

Lin D, Jiang Q, Zheng K, Chen S, Zhou H, Gong X, Xu J, Teng S, Dong Y. 2015. Mutation of the rice *ASL2* gene encoding plastid ribosomal protein L21 causes chloroplast developmental defects and seedling death. *Plant Biology*, **17**, 599-607.

Lu Y, Dai S, Gu A, Liu M, Wang Y, Luo S, Zhao Y, Wang S, Xuan S, Chen X. 2016. Microspore induced doubled haploids production from Ethyl Methanesulfonate (EMS) soaked flower buds is an efficient strategy for mutagenesis in Chinese cabbage. *Frontiers In Plant Science*, **7**, 1780.

Luo T, Luo S, Wagner L. 2013. Virus-induced gene silencing of pea *CHLI* and *CHLD* affects tetrapyrrole biosynthesis, chloroplast development and the primary metabolic network. *Plant Physiology and Biochemistry*, **65**, 17-26.

Masuda T. 2008. Recent overview of the Mg branch of the tetrapyrrole biosynthesis leading to chlorophylls. *Photosynthesis Research*, **96**, 121-143.

Nikulin A, Eliseikina I, Tishchenko S. 2003. Structure of the L1 protuberance in the ribosome. *Nature Structural & Molecular Biology*, **10**, 104–108.

Naing A H, Kyu S Y, Pe P P W. 2019. Silencing of the phytoene desaturase (*PDS*) gene affects the expression of fruit-ripening genes in tomatoes. *Plant Methods*, ***15***, 110.

Ostheimer G J, Williams-Carrier R, Belcher S, Osborne E, Gierke J, Barkan A. 2003. Group II intron splicing factors derived by diversification of an ancient RNA-binding domain. *Embo Journal*, **22**, 3919-3929.

Pesaresi P, Varotto C, Meurer J, Jahns P, Salamini F, Leister D. 2001. Knock-out of the plastid ribosomal protein L11 in *Arabidopsis*, effects on mRNA translation and photosynthesis. *Plant Journal*, **27**, 179-189.

Papenbrock J, Mock H P, Tanaka R, et al. 2000. Role of magnesium chelatase activity in the early steps of the tetrapyrrole biosynthetic pathway. *Plant Physiology*, **122**, 1161-1169.

Polivka T, Frank H A. 2010. Molecular factors controlling photosynthetic light harvesting by carotenoids. *Accounts of Chemical Research*, **43**, 1125-1134.

Robles P, Quesada V. 2022. Unveiling the functions of plastid ribosomal proteins in plant development and abiotic stress tolerance. *Plant Physiology and Biochemistry*, **189**, 35-45.

Romani I, Tadini L, Rossi F, Masiero S, Pribil M, Jahns P, Kater M, Leister D, Pesaresi P. 2012. Versatile roles of *Arabidopsis* plastid ribosomal proteins in plant growth and development. *Plant Journal*, **72**, 922-934.

Schultes N P, Sawers R J H, Brutnell T P, Krueger R W. 2000. Maize mutation is caused by a disruption of the gene encoding the chloroplast ribosomal small subunit protein 17. *Plant Journal*, **21**, 317-327.

Shimoda Y, Ito H, Tanaka A. 2012. Conversion of chlorophyll b to chlorophyll a precedes magnesium dechelation for protection against necrosis in *Arabidopsis*. *Plant Journal*, **72**, 501-511.

Sun Y, Zerges W. 2015. Translational regulation in chloroplasts for development and homeostasis. *Biochimica et Biophysica Acta*, **1847**, 809-820.

Sun X, Li X, Lu Y, Wang S, Zhang X, Zhang K, Su X, Liu M, Feng D, Luo S. 2022. Construction of a high-density mutant population of Chinese cabbage facilitates the genetic dissection of agronomic traits. *Molecular Plant*, **15**, 913–924.

Tanaka R, Tanaka A. 2011. Chlorophyll cycle regulates the construction and destruction of the light-harvesting complexes. *Biochimica et Biophysica Acta - Bioenergetics*, **1807**, 968-976.

Tiller N, Bock R. 2011. The translational apparatus of plastids and its role in plant development. *Molecular Plant*, **7**, 1105-1120.

Wang R, Song H, Zhang W J, Wang N, Zhang S J, Shao R Q, Liu C M. 2023. Structural insights into the functions of *Raf1* and *Bsd2* in hexadecameric Rubisco assembly. *Molecular Plant*, **16**, 1927-1936.

Wang Z, Zhang L, Dong C. 2021. Characterization and functional analysis of phytoene synthase gene family in tobacco. *BMC Plant Biology*, **21**, 32.

Wicke S, Schneeweiss G M, dePamphilis C W, Müller K F, Quandt D. 2011. The evolution of the plastid chromosome in land plants: gene content, gene order, gene function. *Plant Molecular Biology*, **76**, 273-297.

Woodson J D, Joens M S, Sinson A B, Gilkerson J, Salom P A, Weigel D. 2015. Ubiquitin facilitates a quality-control pathway that removes damaged chloroplasts. *Science*, **350**, 450-454.

Yu X, Yu J, Lu Y, Li W, Huo G, Zhang J, Li J. 2024. An efficient and universal protoplast-based transient gene expression system for genome editing in Brassica crops. *Horticultural Plant Journal*, **10(4)**, 983-994.

Yang Y Y, An X H, Rui L, Liu G D, Tian Y, You C X, Wang X F. 2024. *MdSnRK1.1* interacts with *MdGLK1* to regulate abscisic acid-mediated chlorophyll accumulation in apple. Horticulture Research, 11, uhad288.

Zhang J X, Yuan H, Yang Y, Fish T, Zhang LG, Li L. 2016. Plastid ribosomal protein S5 is involved in photosynthesis, plant development, and cold stress tolerance in *Arabidopsis*. *Journal of Experimental Botany*, **67**, 2731-2744.

Zhao M H, Li X, Zhang X X, Zhang H, Zhao X Y. 2020. Mutation mechanism of leaf color in plants, A review. *Forests*, **11**, 8.

Zhao C, Liu L, Safdar L B. 2020. Characterization and fine mapping of a yellow-virescent gene regulating chlorophyll biosynthesis and early stage chloroplast development in *Brassica napus*. *G3-Genes Genomes Genetics*, **10**, 3201-3211.